Remote Sensing Upside Down: Exploring the Potential of Ground-Based Multispectral Cameras for Tree Crown Monitoring

Mona Goebel¹, Lukas Wolf¹, Frederik Packwitz¹, Dorota Iwaszczuk¹

¹ Technical University of Darmstadt, Remote Sensing and Image Analysis group, Germany (mona.goebel@, frederik.packwitz@stud., dorota.iwaszczuk@) tu-darmstadt.de

Keywords: Forest, NDVI, Canopy Openness, Radiometric Quality Assessment

Abstract

Recent advancements in remote sensing have enabled increasingly detailed analysis of forest canopies using a range of platforms, from satellites to ground-based systems. This study focuses on zenith multispectral imaging beneath deciduous tree crowns to assess canopy openness and vegetation activity. We conducted two experiments: First, we evaluated the spectral similarity between a 10-lens multispectral camera and a spectrometer in a controlled environment. Using Spectral Angle Mapping (SAM) and common Vegetation Indices (VIs), we found that reflectance data acquired at 0.5 m distance under diffuse light closely matched spectrometer measurements. Second, we monitored seasonal foliage development between February and July 2025, capturing ground-based reflectance from 400–850 nm. The inclusion of near-infrared (NIR) bands significantly improved the detection of vegetation activity throughout the growth season. Our results indicate that absolute reflectance values from images captured at greater zenith distance are uncertain due to angular and illumination effects, but relative changes between bands remain informative. Among the tested indices, the Green Normalised Difference Vegetation Index (GNDVI) aligned well with reference data and remained unsaturated during peak foliage months.

1. Introduction

Recent advances in remote sensing have significantly enhanced our ability to observe and analyse the Earth's surface, particularly in forestry, which spans about a third of global land. Remote sensing platforms vary in range—from high-altitude satellite sensors and mid-range aircraft systems to close-range platforms like drones, handheld devices, and backpack-mounted sensors that capture fine-scale detail. Each offers distinct advantages depending on the application and scale of observation (Ecke, 2025).

The field of canopy openness is well researched and forest canopy photography has been done since 1960s (Chianucci, 2019). Most work use fish-eye lens with a large field of view, also called hemispherical photography. Canopy analysis can also be divided into down-looking (nadir) and up-looking (zenith) direction. In this research field, most works choose the blue band or a mean grey image as the base for the segmentation of sky and non-sky area. Variations of thresholding has been introduced, concluding that local or region based thresholding is superior to global based. As this research field gained more and more importance, the availability of commercial software grew (Li et al., 2023).

As most approaches use cameras sensitive only to visible light, the discussion of leaf area indices (LAI) often mixes wood and leaf areas. The separation only becomes possible with the introduction of near-infrared (NIR) data (Chianucci, 2019). Most work also estimated the plant state and leaf area on greenness level (Li et al., 2023). A new approach of adding NIR to canopy openness analysis was published by Chapman (2007). He used manual filters for his Nikon Coolpix 950 to separate bands. He also noted the important distinction that satellite-derived pixel values capture sunlight reflected from objects, whereas zenith measurements capture diffuse and transmitted radiation. Zou et al. (2009), who also used manual filters, criticised that im-

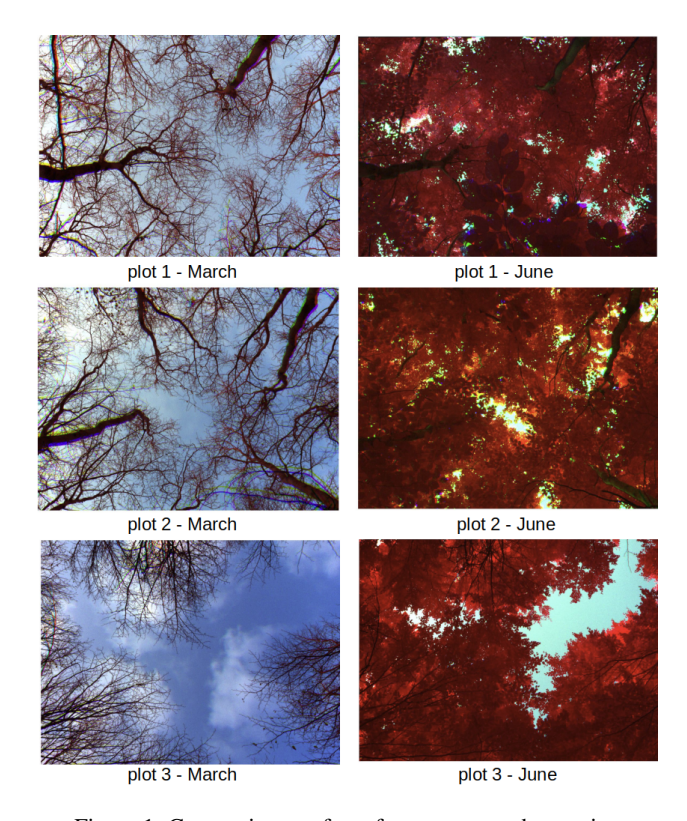


Figure 1. Camera images from forest canopy observation experiment, visualised as coloured-infrared. This excerpt only shows March and June.

ages could not be taken simultaneously as the filter needed to be changed in between captures. The authors analysed the dependency between angular diversions from zenith with the wood and leaf area index. A few years later, Chianucci et al. (2021) analysed the change of canopy parameters with daily RGB images from beneath the canopy in combination with Sentinel-2 imagery to assess phenological observations.

In this study, we first examine the difference in light reflectance captured by a 10-lens multispectral camera and a spectrometer in a controlled environment. Spectral Angle Mapping (SAM) is a common approach to determine the differences of surfaces numerically (Dennison et al., 2004; Jiang et al., 2020; European Space Agency, 2025). We use this measure to analyse how well the reflectance captured by the camera in a controlled setting matches the reflectance captured by the spectrometer. The spectrometer data serves as the reference data in all our experiments. Next to SAM, Vegetation Indices (VIs) are also taken as indication for similarity, as these are common indices and likewise independent to change of brightness. Second, we examine how the inclusion of red-edge and near-infrared (NIR) bands from a 10-lens multispectral camera improves canopy openness and tree condition monitoring. We compare various VIs to analyse their sensitivity to changes in vegetation activity during the growth season. Our research focuses on a small forest area, capturing tree crowns from a zenith perspective below the canopy. Between February and July 2025, we analyse foliage reflectance across wavelengths ranging from 400 to 850 nm.

2. Method

In the first step, the radiometric quality of the camera image pixel values is assessed. We therefore begin in a controlled laboratory setting (Section 2.1) and compare reflectance from stable coloured fields. Thereafter, in a natural forest setting and from tree crown images, foliage pixels are extracted and crown metrics as well as vegetation indices calculated (Section 2.2).

Radiometric Quality Assessment

The radiometric quality is quantified in this work by three types of metrics, which compare multispectral camera image pixel values with reference values. The first metric is Spectral Angle Mapping (SAM) by Kruse et al. (1993):

$$SAM = \cos^{-1} \left(\frac{\sum_{b=1}^{n} C_b^{image} \times C_b^{ref}}{\sqrt{\sum_{b=1}^{n} (C_b^{image})^2} \times \sqrt{\sum_{b=1}^{n} (C_b^{ref})^2}} \right),$$
(1)

where C is the reflectance value per colour band, b is the current band number, n the total band number, image is the reflectance values from image and ref the reflectance values from reference source. This similarity measure is unaffected by gain factors, as vector angles remain constant regardless of magnitude. It therefore allows direct comparison between lab spectra (reference) and remotely sensed reflectance (images). For example, if the image and reference data are identical, then SAM equals 0°. In contrast, if the reflectances are not equal, the highest possible radian angle is SAM = 1.57° (or $\frac{\pi}{2}$).

The second metric is the commonly known Relative Mean Square Error (RMSE):

RMSE =
$$\sqrt{\frac{1}{n} \sum_{b=1}^{n} (C_b^{image} - C_b^{ref})^2}$$
 . (2)

RMSE and SAM correlate as analysed by Dennison et al. (2004).

Lastly, the third type of similarity metric is Vegetation Indices (VIs). We use Normalised Difference Vegetation Index (NDVI) (Rouse et al., 1974), Red Edge NDVI (reNDVI) (Roujean and Breon, 1995) and Normalised Difference Red Edge Index (NDRE) (Gitelson and Merzlyak, 1994):

$$NDVI = \frac{NIR - R}{NIR + R} \tag{3}$$

$$NDVI = \frac{NIR - R}{NIR + R}$$

$$reNDVI = \frac{RE - R}{RE + R}$$

$$NDRE = \frac{NIR - RE}{NIR + RE}$$
(5)

$$NDRE = \frac{NIR - RE}{NIR + RE} \tag{5}$$

where NIR (near-infrared), R (red), RE (rededge) are pixel values in the respective bands. NDVI tends to saturate more quickly than NDRE with respect to chlorophyll concentrations (Gitelson and Merzlyak, 1994) and saturates in dense, multilayered canopy (Haboudane et al., 2004). NDVI shows a nonlinear relationship with LAI values (Haboudane et al., 2004; Delegido et al., 2013).

Values are averaged over pixel values taken within a defined window, as visualised in Figure 3.

2.2 Crown Image Processing

Images taken at zenith direction from forest tree crowns were processed to collect information on crown size and character. First, tree crown images were segmented into sky and non-sky regions. The sky segmentation is using an adaptive threshold based on a local mean filter with a moving window. The following equations 6 to 15 are taken from Alivernini et al. (2018) and adaptions by us are indicated.

From the resulting sky mask, the total sky gaps g_T and large sky gaps g_L are determined. Note, that g_T is equal to all sky pixels. The region size per sky and non-sky needs to be determined first. This is done using NumPy's bincount function, which counts the occurrences of integer values (1 and 0) representing sky and non-sky pixels. The mean region size μ_g and variance σ_g^2 are then computed as follows:

$$\mu_g = \frac{1}{N} \sum_{i=1}^{N} g_i \tag{6}$$

$$\sigma_g^2 = \frac{1}{N} \sum_{i=1}^{N} (g_i - \mu_g)^2 \tag{7}$$

where g_i represents the size of an individual sky region, and Nis the total number of sky regions.

The threshold g^{thresh} between large sky gaps g_L and small sky gaps g_S is defined as:

$$g^{\text{thresh}} = \mu_g + \sqrt{\frac{\sigma_g^2}{N}} + a \tag{8}$$

where $\sqrt{\frac{\sigma_g^2}{N}}$ accounts for the standard error of the mean region size. $g_L>=g^{\rm thresh}$ are large gaps, and $g_S< g^{\rm thresh}$ small gaps. We added the constant a which adds a number of pixels to the dynamic threshold.

The pixel number of large sky gap g_L is computed as:

$$g_L = g_T - g_S \tag{9}$$

Based on these sky gap parameters Crown Cover (CC), Foliage Cover (FC), Crown Porosity (CP), Gap Fraction (GP) and Leaf Area Index (LAI) were computed. Note that FC is a regional subset of CC. LAI_{nc} as the standard approach uses Beer's law (Beer, 1852), assuming random foliage distribution. LAI_c as clumping corrected version accounts for non-random structure.

In the calculation of canopy structure metrics, the following equations are used:

 Crown Cover (CC): Proportion of total pixels occupied by wood and foliage.

$$CC = 1 - \frac{g_L}{p_T} \tag{10}$$

where g_L represents the total number of pixels in large sky gaps, and p_T is the total number of pixels in the image.

2. **Foliage Cover (FC)**: Proportion of total pixels occupied by foliage. FC is by definition smaller than CC.

$$FC = 1 - \frac{g_T}{p_T} \tag{11}$$

where g_T represents the total number of sky pixels.

Crown Porosity (CP): The ratio of foliage cover to crown cover, indicating leaf distribution patterns.

$$CP = \frac{FC}{CC}$$
, if $CC > 0$, otherwise $CP = 0$ (12)

This avoids division by zero in cases where CC = 0.

4. **Gap Fraction (GP)**: The probability of light penetration through gaps in the canopy, or in other words, visibility of sky through gaps within the canopy.

$$GP = \frac{(1-CP) \times \ln(1-FC)}{\ln(CP) \times FC},$$
 if $CP > 0$ and $FC > 0$, otherwise $GP = 0$ (13)

5. Leaf Area Index (LAI) without Clumping Correction (LAI_{nc}): The standard LAI using Beer's law, which assumes a random foliage distribution, is given by:

$$LAI_{nc} = -\frac{\ln(1-FC)}{k},$$
 if $(1-FC) > 0$, otherwise $LAI_{nc} = 0$ (14)

where k is the extinction coefficient, which depends on leaf angle distribution, and set to k=0.5, same as from (Alivernini et al., 2018).

6. Leaf Area Index (LAI) with Clumping Correction LAI_c: The clumping-corrected LAI accounts for nonrandom foliage distribution:

$$LAI_c = -CC \times \frac{\ln(CP)}{k},$$
 if $CP > 0$, otherwise $LAI_c = 0$ (15)

In all equations, if CC or FC are negative or 1, the result was viewed as error and set to zero.

To improve foliage identification, we extended the FC definition using NDVI (Equation (3)). Pixels, which were classified in the first step as non-sky, and hold an NDVI \geq *threshold* were classified as foliage; those below the NDVI threshold as non-foliage.

To analyse the change in leave activity further, two additional vegetation indices are included, besides NDVI, reNDVI and NDRE. The Green Normalized Difference Vegetation (GNDVI) (Gitelson et al., 1996) derived by:

$$GNDVI = \frac{NIR - G}{NIR + G}$$
 (16)

and the Modified Chlorophyll Absorption Ratio Index 2 (MCARI2) (Haboudane et al., 2004) with:

$$MCARI2 = \frac{1.5 \cdot (2 \cdot NIR - 1.3 \cdot RE - 0.7 \cdot B)}{\sqrt{(2 \cdot NIR + 1)^2 - 6 \cdot NIR + 5 \cdot \sqrt{R} - 0.5}},$$
(17)

where B, G, RE and NIR are pixels from the blue, green, rededge and near-infrared band, respectively.

3. Experiments

For all experiments we used the drone camera MicaSense RedEdge MX Dual System, which has comparable spectral bands to the satellite Sentinel 2. Two separate cameras, each with five bands, make up the camera system (Figure 2), along with a Downwelling Light Sensor (DSL2). The 10 individual lenses each have a 47.2° horizontal field of view, a synced global shutter and an automatic exposure time. The camera bands are sensitive in the following electromagnetic wavelengths in nm (band span): coastal blue 444 (28), blue 475 (32), green 531 (14), green 560 (27), red 650 (16), red 668 (14), rededge 705 (10), rededge 717 (12), rededge 740 (18) and near-infrared 842 (57). Notable is the shift in view per lens in the 10-lens camera system at 0.5 m distance (Figure 2 and Figure 3). The raw multispectral images were acquired as one image per band and then aligned and stacked into image size (905, 1220, 10). Reference reflectance values were measured with a CI-710S SpectraVue Leaf spectrometer (CID Bio Science, Inc.), which uses a CMOS linear array sensitive to 200–1100 nm wavelengths with a 3 nm bandwidth. For spectral comparison, the spectrometer bands closest to the camera's were selected, though a bandwidth mismatch remains.

Experiment 1: Radiometric Quality Assessment. In a controlled indoor setting, we placed a ColorChecker Video calibration board (Calibrite LLC) 0.5 m away from the camera under diffuse sunlight (Figure 2). Median pixel values were extracted from each colour field using manually selected 2×2 patches. For the larger grey field on the board's backside, a 15×15 patch was used. All fields were measured with the spectrometer thrice and an average was derived as the final reference data. Its builtin light source illuminated samples for an average of 6 ms. For the Vegetation Indices (VI) calculations, the following bands are used: R = red band 668 nm, RE = red edge band 705 nm, NIR = NIR band 842 nm.

Experiment 2: Forest Canopy Observation. Three plots were selected in an urban forest area in Darmstadt, Germany.

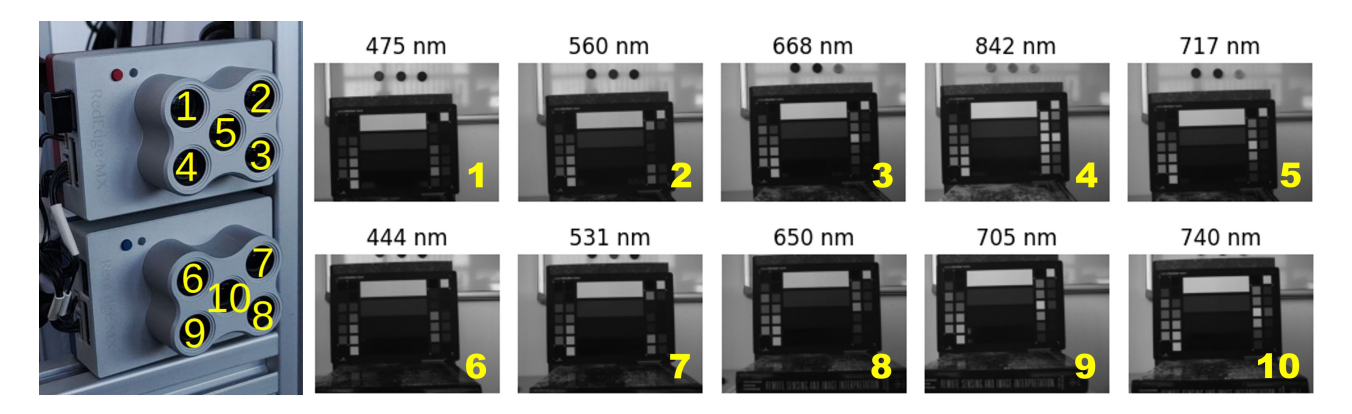


Figure 2. Camera used in all experiments (left) and Colour calibration board (right) visualised per band, sorted by lens order. Yellow numbers indicate original band numbers.

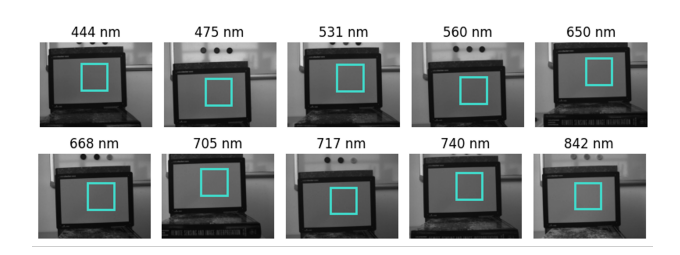


Figure 3. Visualisation of colour calibration board grey field and the corresponding patch area per band. Bands are sorted by wavelengths.

Plot 1 (49.86293367, 8.690704) has the densest canopy, fully covering the image scene; plot 2 (49.86291908, 8.69039499) has less dense cover; and plot 3 (49.86275099, 8.69016504) has the least canopy cover (Figure 1). The plots, located only a few metres apart, contain medium-aged European beech with heights up to 20 m. At this distance, the camera image covers about 17.5 m horizontally. Starting on February 25, 2025, images were taken every four weeks at sunrise. The camera is placed on a tripod at the same position within each plot and 1 m above ground in zenith direction. Note that due to technical failure, for plot 1 and plot 3 in June only camera bands 1-5 (blue 475 nm, green 560 nm red 668 nm, rededge 717 nm and near-infrared 842 nm) could be used. Reference data was only taken during the leaf-on season, visible in these plots from April on. To obtain reference data, one small twig was gathered at a height of 10-12 metres in the tree crown. Three trees were selected per plot and five spectrometer measurements were taken per twig, scattered over several leaves. Spectrometer measurements were conducted seconds after the twig was cut from the tree. In total, 15 measurements were taken per plot and month and then averaged to form the reference data. For tree crown image processing, all images were normalised by excluding the lower and upper 2% percentiles across all channels of each image and stretching the remaining pixel values to the range $\boldsymbol{0}$ -255. Thus, the relative pixel values between channels are unchanged. For the sky segmentation, we used the red band as basis, as it generally shows a strong contrast between sky and living vegetation. During the sky gap threshold determination, we set a = 1000 in Equation (8). Furthermore, we set the vegetation threshold separating foliage and non-foliage for the FC calculation to NDVI > 0.3, as (Carlson and Ripley, 1997; Huete et al., 1997) indicate it to be the lower limit of photosynthetically active green vegetation. For the VI calculations, the bands 1-5 are used: B= blue band 475 nm, G= green band 560 nm, R= red band 668 nm, RE= rededge band 717 nm, NIR= NIR band 842 nm.

4. Results

First, the result of the radiometric quality assessment are presented (Section 4.1) with a visual comparison of signatures (Figure 4) derived from camera image and spectrometer as reference for the colored fields (Figure 2) and as table for the grey field (Table 1). This is supported by numeric comparison of SAM and VIs (Table 2). Second, we present results of the forest canopy observation experiments (Section 4.2), with a data series from February to July over all three plots regarding canopy characteristic (Figure 5), signature evolution (Figure 6) and VIs evolution (Figure 7).

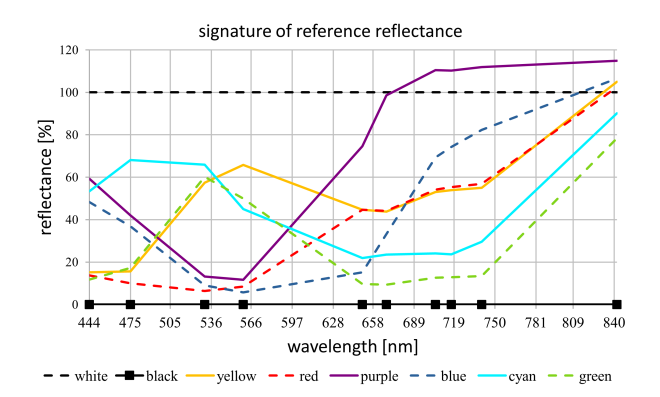
4.1 Radiometric Quality Assessment

On the grey field (Figure 3), the average standard deviation of raw image pixel values within the selected window is 6.67 (6.5 %) (Table 1). The mean image pixel values in the original reflectance signature of the homogeneous grey field is 102 ± 7.6 , and after normalising these values with the respective white and black fields, the average is at 58 ± 5.6 . In comparison, the mean grey value in the reference data is 59 ± 1.1 . With the normalised reflectance values, SAM is 0.1° and RMSE is 9.9 %, which is close to the mean RMSE across the coloured fields.

| band (nm) | 444 | 475 | 531 | 560 | 650 | 668 | 705 | 717 | 740 | 842 |
|-------------------|------|------|------|------|------|------|------|------|------|------|
| camera mean | 99 | 102 | 104 | 94 | 105 | 97 | 111 | 94 | 100 | 118 |
| camera st.d. | 6.6 | 7.0 | 6.6 | 6.6 | 6.6 | 6.6 | 6.7 | 6.9 | 6.2 | 6.9 |
| camera normalised | 55 | 57 | 59 | 54 | 66 | 54 | 59 | 52 | 54 | 69 |
| reference | 61 | 60 | 60 | 60 | 59 | 59 | 58 | 58 | 58 | 57 |
| factor | 1.11 | 1.05 | 1.01 | 1.11 | 0.00 | 1.09 | 0.00 | 1.11 | 1.07 | 0.83 |

Table 1. Reflectance on grey field of colour calibration board. st.d.: standard deviation; normalised: values scaled using white/black fields; Reference: pre-calibrated values from spectrometer; factor = normalised / reference.

All reflectance on the coloured patches were normalised on their respective white and black fields, which is why the lines in Figure 4 are straight for white and black. According to SAM, the reflectance difference is overall similar, with highest spectral difference between image and reference being on the green field (0.09), lowest on the purple field (0.02), and with an overall average of 0.05 (Table 2). The green field is of most interest



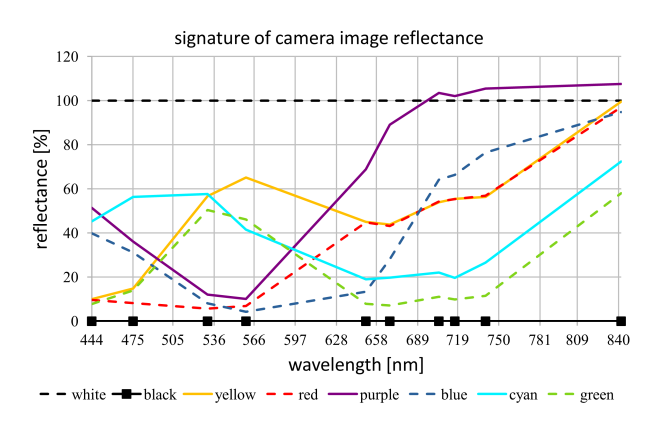


Figure 4. Reflectance signatures from reference (top) and image pixels (bottom) on calibration board colour patches. Values are normalised using black and white fields.

| colour fields | yellow | red | purple | blue | cyan | green | mean |
|---------------|--------|-------|--------|-------|-------|-------|-------|
| SAM (radians) | 0.04 | 0.04 | 0.02 | 0.03 | 0.05 | 0.09 | 0.05 |
| RMSE (%) | 4.22 | 2.61 | 3.72 | 6.37 | 18.39 | 13.80 | 8.24 |
| NDVI diff | 0.02 | 0.01 | -0.02 | -0.02 | 0.01 | 0.01 | 0.00 |
| reNDVI diff | -0.02 | -0.02 | 0.00 | -0.02 | -0.02 | -0.01 | -0.01 |
| NDRE diff | 0.03 | 0.03 | 0.00 | 0.02 | 0.04 | 0.04 | 0.02 |

Table 2. Radiometric quality results. All are normalised on white and black fields. Vegetation Index (VI) diff = $VI_{reference}$ - VI_{image} .

as it aligns with the target objects: green tree leaves. In contrast, RMSE show more variability with the second-highest RMSE value on the green field (13.8 %). For vegetation indices, overall average differences are 0.00 (NDVI), -0.01 (reNDVI), and 0.02 (NDRE).

Notably, the signature on the purple field shows higher reflectance above 700 nm than the white field (Figure 4), a consistent effect across repeated measurements. Above 700 nm, material properties dominate more than visible colour as this is beyond the human visible wavelength, and the calibration board is designed for RGB cameras. This phenomenon is also in the reference data, with addition of NIR values above white in other coloured fields too.

4.2 Forest Canopy Observation

Results for Crown Canopy (CC), Foliage Canopy (FC), Canopy Porosity (CP) and LAI_{nc} without clumping correction are visualised in Figure 5. In February and March, CC values within each plot remain low in these months, and decrease from plot 1 to plot 3 with the expected density decline. Thereafter, the values increase until May and remain stable in June and July in

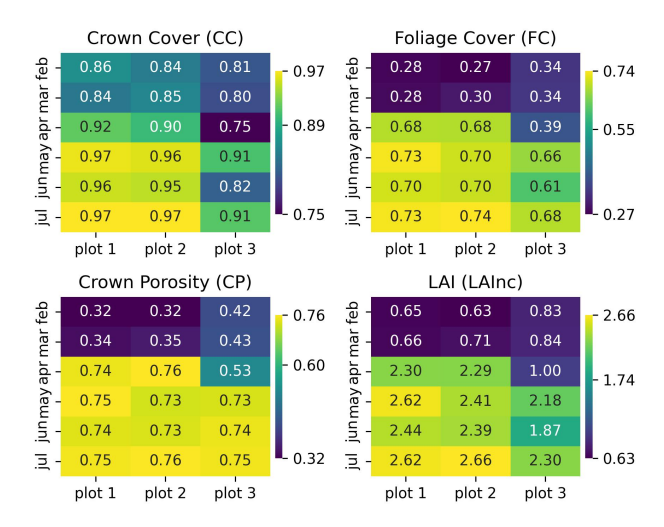


Figure 5. Tree crown segmentation results for metrics CC, FC, CP and LAI_{nc} . Colour scales indicate minimum, maximum and mean values.

plot 1 and plot 2. Only plot 3 shows an unaligned low value in April and June. Overall CC values rise approximately from 0.8 to 1. As the trees do not carry leaves in the winter months, FC values show the expected trend of increasing values towards July. Plot 3 with the lowest crown density holds in winter higher values than plot 1 and plot 2. From April on, plot 3 shows increasing values up until May, but lower than the other two plots. However, as no leaves are on the trees in February and March, an FC value of near zero was expected. Overall the FC values rise approximately from 0.3 to 0.7. The ratio between CC and FC is expressed by CP. While CC remains almost constant over the months, FC increases rapidly. Thus, by definition, CP shows a similar pattern than FC, with overall values rising approximately from 0.3 to 0.7. LAI_{nc} commences in February with around 0.64 in plot 1 and plot 2, meaning little amount of leaves. The values increase to approximately 2.4 with increasing values from plot 3 to plot 1 as the canopy density increases. Further, Gap fraction (GP) and LAI_c with clumping correction indicate more leaves in winter than in spring. In more detail, in February plot 1 and plot 2 begin with 0.7 and increase to 1.56 and 1.48 in May, respectively. Plot 3 increases from 0.82 to 1.41. LAI_c declines from 1.95, 1.91 and 1.40 for plot 1-3 in February to 0.54, 0.61 and 0.57.

The original method of FC calculation by Alivernini et al. (2018), which is solely based on the gap sizes in sky pixels, was replaced by our FC method based on NDVI values of non-sky pixels. In February, our FC is on average over all plots 64% lower than the original method, while in June our FC is on average 27% higher.

Regarding the signature of foliage pixels (Figure 6), the first two months over all plots do not resemble a typical vegetation signature. Signatures are based on all foliage pixels, which are non-sky pixels with NDVI > 0.3. With the growth of leaves, the NIR value (842 nm band) increases and reflectance in visible light decreases relatively, indicating a rise in photosyntheses activity or a reduction of false objects classified as foliage. Beginning from May, the usual dip upwards in the green is notable only in plot 2. In addition, the standard deviation decreases in plot 1 and plot 2 as more pixels are included as the basis for the signature. For example in plot 1 the amount of non-sky pixels with NDVI > 0.3 increases from 28 % to 73 % in May. This

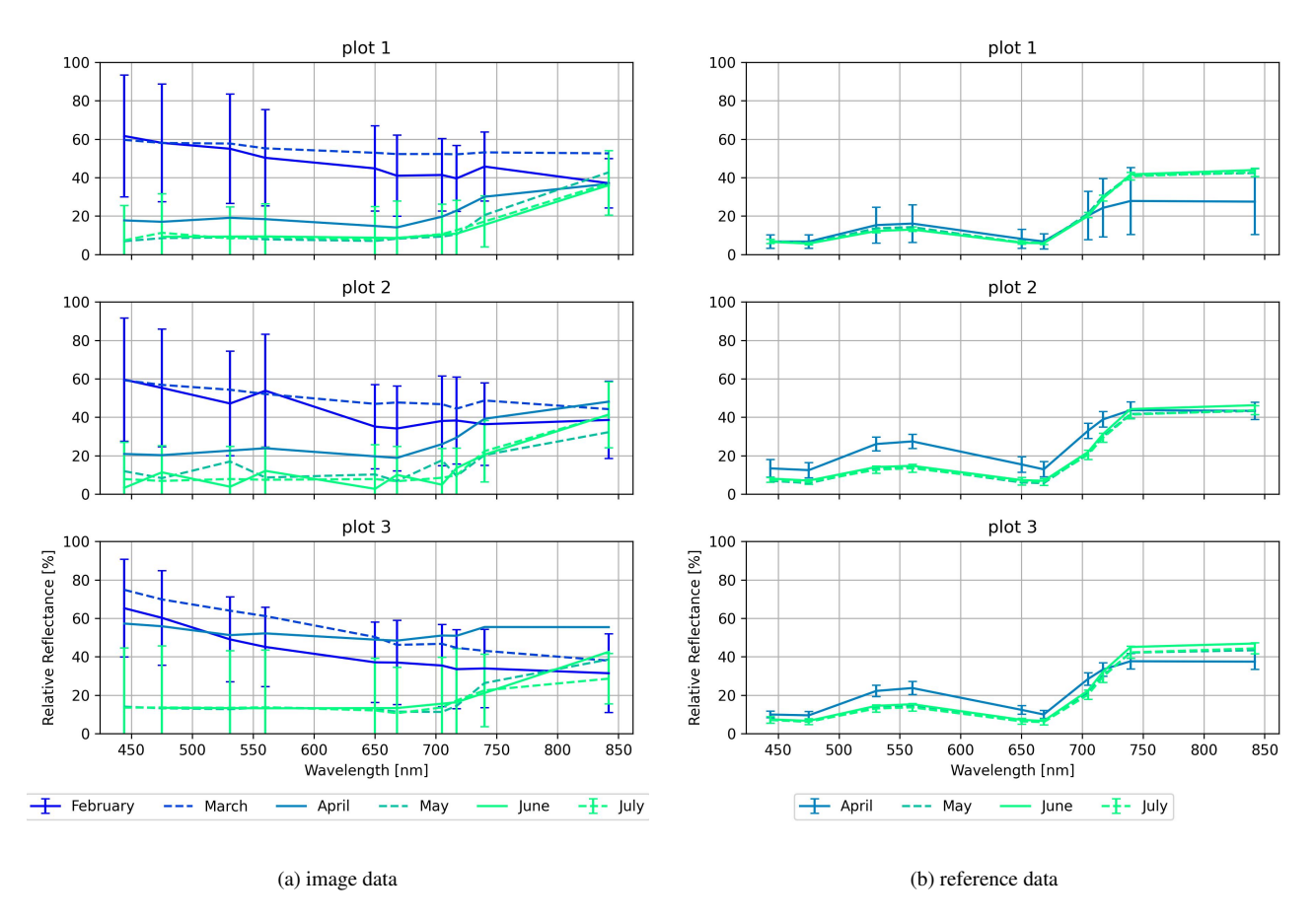


Figure 6. Mean signatures of (a) image data February to July and (b) reference data for leaf-on months April to July. Standard deviation as vertical bars for better visibility only for selected months.

trend is not notable in plot 3 as the standard deviation increases in the visible light from February to July, even though the underlying pixel amount increases from 34 % to 68 %.

Reference leaf measurements could not be taken in February and March as no leaves were present, hence Figure 6 on the right only shows signature from April. The typical contrast between low light reflectance of blue and red with the higher reflectance of green is more prominent in the reference data than the image derived data (Figure 6). Furthermore, rededge values are lower in the leaf-on months in the image derived signature than the reference. Overall, changes between 740 nm and 842 nm are not similar between the images and the reference. SAM between the signatures derived from the images and their reference for plot 1 in April is 0.13°, and 0.55° in May. Note that camera images are not calibrated and absolute numbers vary with changes of absolute light quantity during measurements. In contrast, the reference data is calibrated before each measurement day and is in direct contact with the leaf during measurement, thus the light quantity and direction is stable over all measurements.

The popular NDVI increases from zero to around 0.6 (Figure 7). The reference data is showing higher values between April and July. From April to May, the NDRE derived from camera images increases more than the reference. Then, from May to July, the reference remains stable and the image derived index decreases lightly. A similar trend between camera images and reference is given by reNDVI, but values are shifted by 0.5. GNDVI shows the most similar VI values overall between camera image and reference shows. The steepest increase between

February and May shows MCARI2, however similar values in April and higher in May to July than the reference values. Overall, VIs increase with the growth of leaves, aligning with the significant difference in reflectance signature in Figure 6.

5. Discussion

Radiometric Quality Assessment. When taking the variability of the grey field reflectance, VIs based on bands blue (444 nm), red (560 nm) and rededge (717 nm) should be avoided in our setup. The use of the alternative bands reduces a maximum difference over all VIs from 0.1 to 0.04. To give context regarding SAM, Dennison et al. (2004) tested threshold angles between 0.05° and 0.2° for accepting the classification as an endmember in six vegetation land cover classes. Jiang et al. (2020) found thresholds between 0.02° and 0.1° for various minerals through empiric testing. Thus, our angle values are well in acceptable ranges. Regarding VI, Bannari et al. (1995) state that radiometric deterioration alone can cause a relative error of 9 %, next to error source of spectral responses of the sensors. During multiple measurements using the spectrometer an average standard deviation of 0.02 for NDVI values was apparent, before all triplets were summarised into one mean value as reference signature. Therefore, a maximum difference of 0.04 and average of 0.02 between image and reference values over all VIs is good.

Forest Canopy Observation. Crown parameters CC, FC, CP, GP and LAI cannot be compared to related work, as they depend heavily on the individual scene. CC, FC, CP and LAI_{nc}

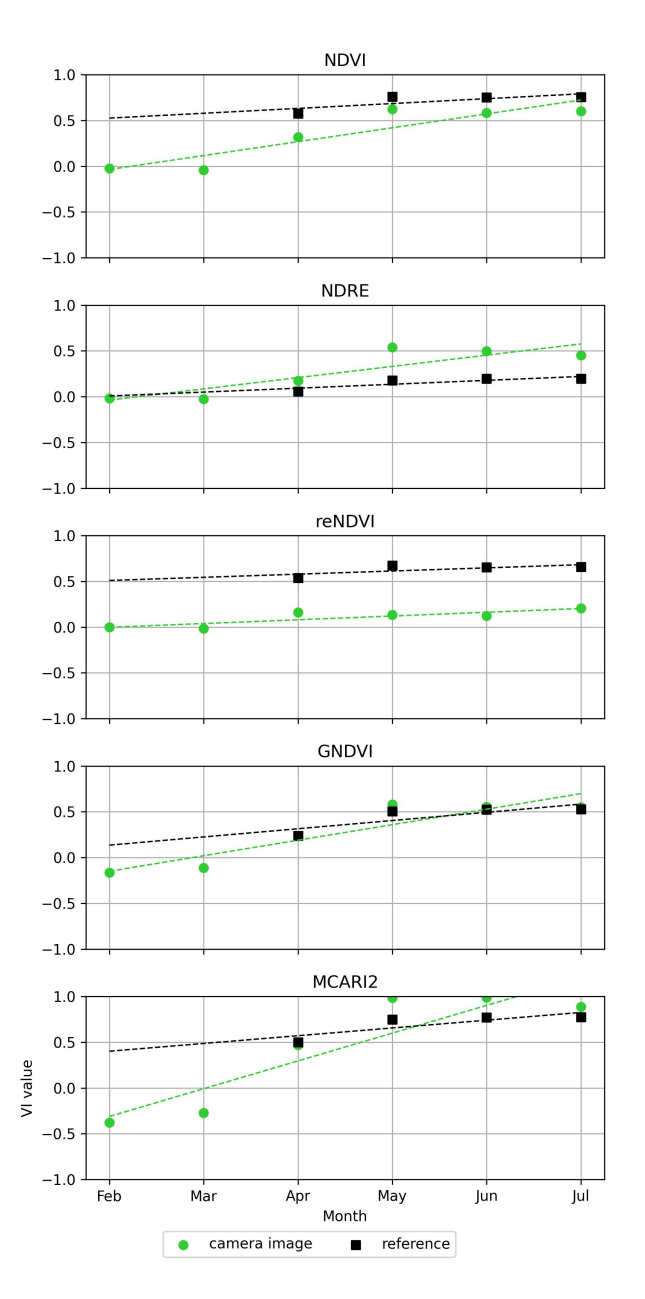


Figure 7. Change of Vegetation Indices (VI) with dashed trend-lines of image and reference data . Reference data collection began in April. VI values derived from mean values in Figure 6 and averaged over plots 1-3.

show an expected trend, aligning with visual interpretation of the evolving scenes. GP and LAI_c however do not. An explanation could be that due to the use of CP in these equations, errors in CC and FC may accumulate. Another explanation could be a false choice of the extinction coefficient *k* more prominent in LAI_c than LAI_{nc}. When comparing the FC calculation based on sky gaps (Alivernini et al., 2018) and our FC calculation based on NDVI, both overestimate a winter scene but ours much less than the gap based method. Our method detects emerging foliage sooner due to its sensitivity to NDVI rather than gap size alone. Camera bands were aligned in post-processing, leading to small mismatches on thin branches and near objects. This can lead to false NDVI values. This is underlined by the foliage signature (Figure 6) based on pixels declared as foliage in February and March. These signatures do not seem to

be typical foliage signatures with a low reflection in blue and red, slightly higher in green and a rapid increase towards nearinfrared wavelengths. The biggest uncertainty is the change of sunlight and light direction. Images in May, June and July were taken under full canopy cover and notably less light was reaching forest ground than previous months. An adjustment in aperture was needed to not underexpose the image. The amount of light under the canopy is a major uncertainty which can lead to more errors during image processing. Especially leaves, which absorb most of the blue and red wavelengths, appeared almost black in images from these three months. However, calibration is difficult, as the calibration field would need to be at the same height as most of the crown, approximately 12 to 25 m, and remain free of leaf cover. The camera image derived signatures show a high standard deviation which suggests a high uncertainty. SAM values between tree crown images and leaf spectrometer data surpass acceptable angles of 0.2°. Regarding Vegetation Indices (VI) as an indication of plant activity, GNDVI and MCARI2 show the greatest change between leafoff and leaf-on season, with the former showing near identical values as the reference. NDVI values where excluded below 0.3 in preprocessing and all VIs were calculated after this exclusion, limiting this analysis.

6. Conclusion

The present study demonstrated the utilisation of ground-based reflectance measurements obtained using a multispectral drone camera. Zenith images were captured from beneath deciduous tree crowns from February to July. In a controlled environment, we demonstrated that reflectance data from multispectral images taken at a distance of 0.5 m with diffuse sunlight are comparable with spectrometer data obtained directly on the object under artificial lighting. Moreover, including the near-infrared band significantly improved the detection of foliage cover over the growing season. Trends in foliage growth and increased vegetation activity could be captured using a 10-lens camera. However, as the experiment results indicate, absolute values from tree crown imagery taken at zenith and approx. 15 m distance cannot be relied upon, hence analysis should target relative changes between bands only. Vegetation indices (VIs) can be used to express vegetation activity, regardless of brightness and gain. In our experiments, the Green Normalised Difference Vegetation Index (GNDVI) showed the most promising results, being close to the reference values and not saturated in May, June and July. We conclude that extending to bands sensitive to non-visible light should be standard practice in canopy openness assessments, especially given the availability of off-theshelf cameras. In future work, a calibration of camera images set in the zenith direction needs to be implemented. Lastly, using these terrestrial images as detailed, punctual reference data for satellite data could be a research target.

7. Acknowledgements

This study is part of the project "Forest health: Interactions of biological, chemical and physical soil parameters with the canopy" funded by the Technical University of Darmstadt. Special thanks is owed to Kai Nitzsche and Collin Weber from the Institute of Applied Geosciences at the Technical University of Darmstadt. Their assistance in the monthly collection of twigs from the treetops was indispensable. Finally, we thank Michael Heethoff and Katja Wehner, from the Biology Department at the Technical University of Darmstadt, for the organisation and coordination regarding the forest plots.

References

- Alivernini, A., Fares, S., Ferrara, C., Chianucci, F., 2018. An objective image analysis method for estimation of canopy attributes from digital cover photography. *Trees*, 32(3), 713–723. DOI: 10.1007/s00468-018-1666-3.
- Bannari, A., Morin, D., Bonn, F., and, A. R. H., 1995. A review of vegetation indices. *Remote Sensing Reviews*, 13(1-2), 95–120. https://doi.org/10.1080/02757259509532298.
- Beer, A., 1852. Bestimmung der Absorption des rothen Lichts in farbigen Flüssigkeiten. *Annalen der Physik*, 162(5), 78–88.
- Carlson, T. N., Ripley, D. A., 1997. On the relation between NDVI, fractional vegetation cover, and leaf area index. *Remote Sensing of Environment*, 62(3), 241-252. https://doi.org/10.1016/S0034-4257(97)00104-1.
- Chapman, L., 2007. Potential applications of near infra-red hemispherical imagery in forest environments. *Agricultural and Forest Meteorology*, 143(1-2), 151–156.
- Chianucci, F., 2019. An overview of in situ digital canopy photography in forestry. *Canadian Journal of Forest Research*, 227–242. https://cdnsciencepub.com/doi/pdf/10.1139/cjfr-2019-0055.
- Chianucci, F., Bajocco, S., Ferrara, C., 2021. Continuous observations of forest canopy structure using low-cost digital camera traps. *Agricultural and Forest Meteorology*, 307, 108516.
- Delegido, J., Verrelst, J., Meza, C., Rivera, J., Alonso, L., Moreno, J., 2013. A red-edge spectral index for remote sensing estimation of green LAI over agroecosystems. *European Journal of Agronomy*, 46, 42-52. https://doi.org/10.1016/j.eja.2012.12.001.
- Dennison, P. E., Halligan, K. Q., Roberts, D. A., 2004. A comparison of error metrics and constraints for multiple endmember spectral mixture analysis and spectral angle mapper. *Remote Sensing of Environment*, 93(3), 359-367. https://doi.org/10.1016/j.rse.2004.07.013.
- Ecke, S., 2025. Drone remote sensing for forest health monitoring. PhD thesis, Albert-Ludwigs-Universität Freiburg. DOI: 10.6094/UNIFR/262641.
- European Space Agency, 2025. Spectral angle mapper (sam) processor. https://step.esa.int/main/wp-content/help/versions/9.0.0/snaptoolboxes/org.esa.s2tbx.s2tbx.spectral.angle.mapper.ui/sam/SAMProcessor.html. ESA SNAP toolbox documentation; accessed June 2025.
- Gitelson, A. A., Kaufman, Y. J., Merzlyak, M. N., 1996. Use of a green channel in remote sensing of global vegetation from EOS-MODIS. *Remote Sensing of Environment*, 58(3), 289-298. https://doi.org/10.1016/S0034-4257(96)00072-7.
- Gitelson, A., Merzlyak, M. N., 1994. Spectral Reflectance Changes Associated with Autumn Senescence of Aesculus hippocastanum L. and Acer platanoides L. Leaves. Spectral Features and Relation to Chlorophyll Estimation. *Journal of Plant Physiology*, 143(3), 286-292. https://doi.org/10.1016/S0176-1617(11)81633-0.

- Haboudane, D., Miller, J. R., Pattey, E., Zarco-Tejada, P. J., Strachan, I. B., 2004. Hyperspectral vegetation indices and novel algorithms for predicting green LAI of crop canopies: Modeling and validation in the context of precision agriculture. *Remote Sensing of Environment*, 90(3), 337-352. https://doi.org/10.1016/j.rse.2003.12.013.
- Huete, A., Liu, H., Batchily, K., van Leeuwen, W., 1997. A comparison of vegetation indices over a global set of TM images for EOS-MODIS. *Remote Sensing of Environment*, 59(3), 440-451. https://doi.org/10.1016/S0034-4257(96)00112-5.
- Jiang, T., van der Werff, H., van der Meer, F., 2020. Classification Endmember Selection with Multi-Temporal Hyperspectral Data. *Remote Sensing*, 12(10). https://www.mdpi.com/2072-4292/12/10/1575.
- Kruse, F., Lefkoff, A., Boardman, J., Heidebrecht, K., Shapiro, A., Barloon, P., Goetz, A., 1993. The spectral image processing system (SIPS)—interactive visualization and analysis of imaging spectrometer data. *Remote Sensing of Environment*, 44(2), 145-163. https://doi.org/10.1016/0034-4257(93)90013-N. Airbone Imaging Spectrometry.
- Li, L., Mu, X., Jiang, H., Chianucci, F., Hu, R., Song, W., Qi, J., Liu, S., Zhou, J., Chen, L., Huang, H., Yan, G., 2023. Review of ground and aerial methods for vegetation cover fraction (fCover) and related quantities estimation: definitions, advances, challenges, and future perspectives. *ISPRS Journal of Photogrammetry and Remote Sensing*, 199, 133–156.
- Roujean, J.-L., Breon, F.-M., 1995. Estimating PAR absorbed by vegetation from bidirectional reflectance measurements. *Remote Sensing of Environment*, 51(3), 375-384. https://doi.org/10.1016/0034-4257(94)00114-3.
- Rouse, J. W., Haas, R. W., Schell, J. A., Deering, D. W., Harlan, J. C., 1974. Monitoring the vernal advancement and retrogradation (greenwave effect) of natural vegetation. Type iii final report, NASA/GSFCT, Greenbelt, MD, USA.
- Zou, J., Yan, G., Zhu, L., Zhang, W., 2009. Woody-to-total area ratio determination with a multispectral canopy imager. *Tree physiology*, 29(8), 1069–1080.